Synchronized Data-Based Identification of Electromechanical Oscillation Modes Using Improved FastICA Considering Measurement Noise

Lixin Wang[1], Binyan Wang[1], Han Gao[2], Deyou Yang[2], Shiwei Xia[3], Tek Tjing Lie[4]

***Abstract*—Synchrophasor-based identification of low-frequency oscillation is an effective means for monitoring the security and stability of power systems, while the loss of identification accuracy due to measurement noise remains a major obstacle. This paper proposes an improved fast independent component analysis (improved FastICA) algorithm to identify oscillation modes (oscillation frequency and damping ratio) from noise-contaminated synchronized measurements. To improve the ability of conventional FastICA to extract modes from noise-polluted synchrophasor, nonlinear matching pursuit (NMP) is introduced to replace the negative entropy calculation of mono-frequency modes in FastICA. NMP enables FastICA to identify oscillation frequency and damping ratio even under strong noise conditions, thereby significantly improving identification accuracy. The performance of the proposed method is evaluated on synthetic signals and numerical simulation signals from IEEE 16-machine system. The results of the identified modes in all cases as well as comparison results from conventional FastICA, EMD and VMD, all combined with Hilbert transform, confirm the accuracy, robustness and efficiency of the proposed method for oscillation mode identification.**

***Index Terms*—low-frequency oscillation, electromechanical modes, improved fast independent component analysis (FastICA), nonlinear matching pursuit (NMP), synchrophasor measurements.**

I. INTRODUCTION

Electromechanical oscillations have become one of the key factors affecting the stability of power systems and limiting the power exchange capability between different regions. Moreover, insufficient damping of oscillation modes can lead to oscillations with growing amplitudes, which may cause power system oscillation instability or even collapse. Therefore, the analysis of electromechanical oscillations is of great significance for maintaining the safe and stable operation of power systems [1].

This work was supported by the State Key Laboratory of Alternate Electrical Power System with Renewable Energy Sources (Grant No. LAPS24014).

Lixin Wang and Binyan Wang are with the School of Electrical Engineering, Northeast Electric Power University, Jilin 132012, China (e-mail: wanglxnedu@163.com; wbinyan2019@163.com); Han Gao and Deyou Yang are with the School of Electrical and Electronic Engineering, Harbin University of Science and Technology, Harbin 150080, China (Hannah 0323gh@hotmail.com; dyyang@hrbust.edu.cn); Shiwei Xia is with the China State Key Laboratory of Alternate Electrical Power System with Renewable Energy Sources(North China Electric Power University), Beijing 101149, China (e-mail: s.w.xia@ncepu.edu.cn); Tek Tjing Lie is with the Department of Electrical and Electronic Engineering, Auckland University of Technology (AUT), Auckland 1010, New Zealand (e-mail: tek.lie@aut.ac.nz).

The oscillation frequency and damping ratio are the two core indicators for evaluating electromechanical oscillations. For the identification of the modes (that is, oscillation frequency and damping ratio), traditionally, oscillation modes are generally obtained by linearizing the nonlinear differential equations of the power system at the equilibrium point [2]. However, with the continuous expansion of power grid and intermittency of renewable generation resources, electromechanical oscillations exhibit complex spatiotemporal characteristics, making it difficult to analyze their parameters. With the widespread use of phase measurement units (PMUs) in real-time monitoring and control techniques for large power grids, it has become feasible to analyze electromechanical oscillations using measurements [3]. For this reason, Power System Dynamic Performance Committee of the IEEE has established a special committee and published some special reports, to discuss mode parameter identification [4].

In recent years, numerous methods have been applied to estimate electromechanical oscillation modes using the measurement data provided by PMUs. Among the many methods published in the past decades, due to the limited PMU configurations available in the early days, the single-channel measurement method was used to identify the oscillation parameters. Representative methods include, such as the widely used Prony method [5] and its improved version [6], the Hilbert-Huang Transform method [7], wavelet method [8], and the TLS-ESPRIT [9]. However, single-channel measurement methods have limitations, as they can only utilize a single measurement signal and may not always achieve optimal observability of dominant modes. Consequently, extracting multiple dominant modes simultaneously using a single signal is often infeasible. Furthermore, there may be bias between the modes extracted using different measurement channels. Recently, with advancements in PMUs and the widespread adoption of wide-area monitoring systems (WAMS) in power systems, the multi-channel measurement-based identification methods have gained popularity for performing modal analysis from the global perspective. Ref [10] proposed a synthetic modal parameter identification (SMPI) method, which combines the stochastic subspace identification method with the Prony method to extract oscillation modes from PMU measurements. Ref [11] proposed a multivariate empirical mode decomposition (MEMD) method, using measurement to identify inter-area modes. Ref [12] proposed an optimal mode decomposition (OMD) method,

which can extract mode parameters from noise-contained measurements. The improved analytical modal decomposition (IAMD) method [13], the multivariate variational mode decomposition (MVMD) method [14], and the stochastic subspace identification (SSI) method [15] are capable of extracting oscillation frequencies and damping ratios from multiple PMUs mounted at different locations.

Blind source separation (BSS) technique is applied as an important modal decomposition tool for PMU measured signals. In the early days, principal component analysis (PCA) achieved linear dimensionality reduction by maximizing variance, providing a preprocessing framework for BSS problems [16,17]. Its core idea is to use second-order statistics (covariance) to find uncorrelated principal components, while it cannot guarantee the statistical independence of the decomposed components, resulting in limited source separation ability. As an extension of PCA technology, independent component analysis (ICA) realizes independent component separation by introducing higher-order statistics to maximize the non-Gaussianity of signals. This overcomes the limitation of PCA relying solely on second-order statistics, enabling BSS to effectively decompose multi-mode coupled signals from PMU measurements [18].

As a fast implementation of ICA, fast independent component analysis (FastICA) method is one popular approach to solve BSS problem and has emerged in recent years as a BSS-based technique for extracting oscillation parameters. Based on its iterative principle, FastICA searches for the target source in the direction of maximum negative entropy to recover the desired source signals from mixed observation measurement signals [19,20]. Moreover, the FastICA algorithm is an effective improvement in suppressing mode aliasing, such as in EMD. However, measurement noise has not been given sufficient consideration in FastICA. Noise interference remains one of the main challenges FastICA faces when applied to the accurate extraction of oscillation parameters from actual PMU measurements. Therefore, how to effectively reduce the impact of measurement noise and reliably identify mono-frequency modes from complex, multi-mode coupled measurements remains an open question.

Motivated by the conventional FastICA algorithm and the nonlinear matching pursuit (NMP) algorithm, this work develops an improved FastICA based data-driven approach. In this work, the negative entropy-based source signal decomposition in conventional FastICA is replaced with the NMP algorithm to accurately extract the oscillation frequency and damping ratio from noise-contaminated PMUs. After modal decomposition, the Hilbert transform (HT) technique is adopted to track instantaneous modal parameters of different modes. This contribution is crucial for accurately identifying the dynamics of electromechanical oscillations without mode mixing from time-series PMU measurement datasets containing noise. The major contributions of this work are as follows:

(1) An improved FastICA-based method for mode parameter identification is proposed. In this method, nonlinear matching pursuit is used instead of negative entropy to extract intrinsic mode function (IMF) so as to obtain the oscillation parameters (that is, oscillation frequency and damping ratio). The decomposition process is simplified and it effectively solves the problem of critical mode information loss caused by measurement noise in conventional FastICA.

(2) Comprehensively considering the influence of inertia and generation capacity on the electromechanical mode information contained in the measurements, an optimal input signal selection strategy based on the capacity-inertia ratio (CIR) index is proposed.

(3) Instantaneous amplitude entropy (IAE), which describes the sufficiency of mode decomposition through the entropy variation, has clear physical significance. In our work, it is applied for the first time to determine the number of dominant modes in mode identification, and to assist FFT in determining the required initial frequency for improved FastICA method.

(4) The effectiveness and superiority of the proposed method for identifying oscillation modes are verified through synthetic signals, simulated data of 16-machine 5-area test system and actual measurement data.

The remainder of this paper is organized as follows. Section II introduces the theoretical background of the low-frequency oscillation and conventional FastICA. Section III develops an improved FastICA-based oscillation modes identification. Section IV describes the implementation of improved FastICA to identify oscillation modes and elaborates on its two critical aspects. Section V evaluates performance of the proposed method using synthetic signals and simulated data. Section VI concludes the paper.

II. Theoretical Background

This section introduces the formulation of low-frequency oscillation decomposition and FastICA algorithm.

A. Low-frequency oscillation decomposition in power systems

A ringdown low-frequency oscillation signal can be regarded as a sum of exponentially damped sinusoids, which is expressed as follows [21]:

$$x(t)=\sum_{k=1}^{N} A_k \underbrace{e^{-\sigma_k t}\sin(2\pi f_k+\varphi_k)}_{s_k(t)} \tag{1}$$

where A_k, σ_k, f_k and φ_k are, respectively, the amplitude, damping coefficient, oscillation frequency and phase of the k-th mode of oscillation signal $x(t)$; N is the number of modes contained in the signal; $s_k(t)$ is the k-th mode.

For multiple measured signals at different nodes in the system, we can construct an input signal matrix $\boldsymbol{X}$, which is expressed as $\boldsymbol{X}=[x_1(t),x_2(t),\cdots,x_M(t)]^{\mathrm{T}}$, where each row corresponds to a measurement channel, and each column represents the sampling points of each measurement channel at the corresponding sampling time; $\boldsymbol{X}$ can be regarded as the linear mixture of amplitude modulated signals, $\boldsymbol{S}=[s_1(t),s_2(t),\cdots,s_N(t)]^{\mathrm{T}}$, which can be expressed as:

$$\boldsymbol{X}=\boldsymbol{A}*\boldsymbol{S} \tag{2}$$

where $\boldsymbol{A}$ is the mixing matrix, its elements correspond to the amplitudes of each mode in the measured signal.

In power systems, $\boldsymbol{X}$ can be collected from PMUs installed on the generators. The aim of measurement-based modes identification is to identify the parameters of $\boldsymbol{S}$ from measurements $\boldsymbol{X}$ in Eq. (2), where $\boldsymbol{A}$ and $\boldsymbol{S}$ are both unknown, so that the mode parameters (oscillation frequency, damping ratio) can be identified from $\boldsymbol{S}$. This is a typical blind source separation (BSS) problem. The basic idea of BSS methods is to determine a de-mixing matrix $\boldsymbol{W}$ for Eq. (2) to separate the source signal $\boldsymbol{S}$ from the observed signal $\boldsymbol{X}$, which is:

$$\boldsymbol{S} \approx \boldsymbol{Y} = \boldsymbol{W} * \boldsymbol{X} \tag{3}$$

where $\boldsymbol{Y}$ is the approximate solution of $\boldsymbol{S}$.

B. Fast Independent Component Analysis (FastICA)

FastICA is a popular approach to solve BSS problem, which realizes the separation of mixed signals based on high-order statistical characteristics. Compared with the other BSS methods, FastICA algorithm does not involve the selection of parameters and can use any nonlinear function to obtain non-Gaussian independent signals with fast convergence speed. The decomposition in FastICA is based on the fixed-point iterative optimization, which continuously optimizes Eq. (3) through the iteration method to make the approximate solution $\boldsymbol{Y}$ closer to the source signal $\boldsymbol{S}$, thereby achieving source signal recovery. Usually, the maximum negative entropy is adopted as the search direction to ensure that the separated signals have the maximum non-Gaussian property.

The negative entropy can be expressed as [22]:

$$N(\boldsymbol{Y}) = H(\boldsymbol{Y}_G) - H(\boldsymbol{Y}) \tag{4}$$

where $H(\mathbf{.})$ represents differential entropy calculation; $\boldsymbol{Y}_G$ and $\boldsymbol{Y}$ are Gaussian distribution vectors with the same variance; $N(\boldsymbol{Y})$ represents the negative entropy of the approximate solution $\boldsymbol{Y}$.

In practical applications, Eq. (5) is usually adopted for approximate calculation:

$$N(\boldsymbol{Y}) = \left\{E\left[g(\boldsymbol{Y})\right] - E\left[g(\boldsymbol{Y}_G)\right]\right\}^2 \tag{5}$$

where $g(\mathbf{.})$ is a nonlinear function; $E(\mathbf{.})$ is the mean function.

The core of separating source signals is to maximize non-Gaussianity as much as possible. Thus, the FastICA algorithm aims to find a matrix $\boldsymbol{W}$ that maximizes the non-Gaussian property of $\boldsymbol{W}^{\mathrm{T}}\boldsymbol{X}$, which should be satisfied as follows:

$$E[\boldsymbol{X}g(\boldsymbol{W}^{\mathrm{T}}\boldsymbol{X})] + E[\boldsymbol{W}^{\mathrm{T}}\boldsymbol{X}g(\boldsymbol{W}^{\mathrm{T}}\boldsymbol{X})]\boldsymbol{W} = 0 \tag{6}$$

The Newton's iteration is applied to Eq. (6), the approximate Newton iteration formula for the de-mixing matrix $\boldsymbol{W}$ is:

$$\begin{cases} \boldsymbol{W}_i^* = E\left[\boldsymbol{X}g(\boldsymbol{W}_i^{\mathrm{T}}\boldsymbol{X})\right] - E\left[g'(\boldsymbol{W}_i^{\mathrm{T}}\boldsymbol{X})\right]\boldsymbol{W}_i \\ \boldsymbol{W}_i = \boldsymbol{W}_i^* / \left\|\boldsymbol{W}_i^*\right\| \end{cases} \tag{7}$$

where $\boldsymbol{W}_i$ is the i-th row of the de-mixing matrix $\boldsymbol{W}$; $\|.\|$ represents the calculation of the norm.

III. Improved FastICA and Electromechanical Oscillation Mode Identification

According to Section II.B, FastICA seeks to maximize negative entropy through iterative optimization using a fixed-point algorithm. However, FastICA is prone to getting trapped in local optima during the iterative process and negative entropy is sensitive to noise, resulting in decreased decomposition accuracy. To this end, nonlinear matching pursuit (NMP) method proposed by Hou and Shi is used to handle the noise in the measurement data and avoid iterative optimization.

A. Improved FastICA

The innovation of NMP also employs a greedy optimization algorithm to calculate de-mixing matrix so as to extract intrinsic mode function (IMF), in particular, NMP has a rigorous mathematical foundation and decomposes the input signal into only a few IMFs. The process of NMP for solving the de-mixing matrix thereby obtaining IMFs is given as follows [23].

Construct a complete dictionary, which is:

$$\boldsymbol{D} = \left\{a(\theta)\cos(\theta) : a \in \boldsymbol{V}(\theta), \theta' \in \boldsymbol{V}(\theta), \theta'(t) \geq 0\right\} \tag{8}$$

where θ is the phase of IMF; $\boldsymbol{V}$ represents the vector space of θ.

In the dictionary $\boldsymbol{D}$, decomposition of the observed signal $x(t)$ is carried out by solving the following minimization problem:

$$\min_{a_i,\theta_i} N$$
$$s.t.\ x(t) = \sum_{i=1}^{N} a_i(\theta_i)\cos\theta_i,\ a_i\cos\theta_i \in \boldsymbol{D}, \forall i \in 1,...,N \tag{9}$$

Considering the noise contained in the measured signal, Eq. (9) is further generalized to Eq. (10) [24]:

$$\min_{a_i,\theta_i} N$$
$$s.t.\ \left\| x(t) - \sum_{i=1}^{N} a_i(\theta_i)\cos\theta_i \right\|_2 \leq \delta,\ a_i\cos\theta_i \in \boldsymbol{D}, \forall i \in 1,...,N \tag{10}$$

where δ is the noise threshold value.

During the decomposition of $x(t)$ into IMFs, an initial guess of the phase θ_i (or angular frequency ω_i=dθ_i/dt) is necessary. Then the i-th IMF obtained by NMP is denoted as:

$$s_i(t) = \mathrm{NMP}(\boldsymbol{x}, \theta_i) = a_i(t)\cos(\theta_i(t)) \tag{11}$$

Next, to obtain the de-mixing matrix $\boldsymbol{W}$ in FastICA, we fully utilize NMP and integrate it with projection pursuit. Our goal is to find the direction $\boldsymbol{W}_i$ such that $\boldsymbol{W}_i\boldsymbol{X}$ corresponds to an IMF s_i with maximum non-Gaussianity, and it should satisfy that $\boldsymbol{W}_i\boldsymbol{X}$ is the same as the IMF obtained through NMP. Thereby, for the first extracted IMF, the following equation should be satisfied:

$$s_1^{\mathrm{T}} = \mathrm{NMP}(\boldsymbol{W}_1^{\mathrm{T}}\boldsymbol{X}, \theta_1) \approx \boldsymbol{W}_1^{\mathrm{T}}\boldsymbol{X} \tag{12}$$

Applying the pseudoinverse of $\boldsymbol{W}_1$ to both sides gives:

$$\boldsymbol{W}_1\mathrm{NMP}(\boldsymbol{W}_1^{\mathrm{T}}\boldsymbol{X}, \theta_1) \approx \boldsymbol{X} \tag{13}$$

We minimize the difference between the two sides of Eq. (13), and $\boldsymbol{W}_1$ can be obtained:

$$\boldsymbol{W}_1 = \arg\min_{\boldsymbol{\omega}} \left\|\boldsymbol{\omega}\mathrm{NMP}(\boldsymbol{\omega}^{\mathrm{T}}\boldsymbol{X}, \theta_1) - \boldsymbol{X}\right\|_2^2,\ s.t.\ \left\|\boldsymbol{\omega}\right\|_2 = 1 \tag{14}$$

Similar to Eq. (12)-Eq. (14), the minimization problem is solved to obtain the de-mixing matrix $\boldsymbol{W}_i$, which is:

$$\boldsymbol{W}_i = \arg\min_{\boldsymbol{\omega}} \left\|\boldsymbol{\omega}\mathrm{NMP}(\boldsymbol{\omega}^{\mathrm{T}}\boldsymbol{R}_{i-1}, \theta_i) - \boldsymbol{R}_{i-1}\right\|_2^2$$
$$s.t.\ \left\|\boldsymbol{\omega}\right\|_2 = 1,\ \boldsymbol{R}_i = \boldsymbol{X} - \sum_{k=1}^{i} a_k s_k^{\mathrm{T}} \tag{15}$$

Then, the *i-th* IMF s_i can be obtained:

$$s_i = \mathrm{NMP}(\boldsymbol{W}_i^{\mathrm{T}}\boldsymbol{R}_{i-1}, \theta_i) \tag{16}$$

According to Eq. (15) and Eq. (16), the solution is iteratively updated, refining the de-mixing matrix $\boldsymbol{W}_i$ and modal component s_i until the maximum decomposition number K is satisfied. Once the condition is satisfied, the mode decomposition results are obtained, yielding K IMFs.

Remark: When the improved FastICA method is applied to decompose the oscillation signal, the number of decomposition (K) plays a crucial role. If K is set to be greater than the actual number of IMFs, the results will include spurious modes; Conversely, if K is set too small, the signal will be insufficiently decomposed, and the components may contain more than two modes. The above situation significantly demonstrates the influence of the number of modes on the identification results. This issue will be further addressed in Section IV.B.

B. Parameter Identification

Perform the Hilbert transform on the mono-frequency mode $s_i(t)$ obtained by improved FastICA, which is [25]:

$$s_i^*(t) = \frac{1}{\pi} P \int_{-\infty}^{+\infty} \frac{s_i(\tau)}{t-\tau} d\tau \tag{17}$$

where P is the principal Cauchy integral value.

Then, the analytic signal of $s_i(t)$ is constructed as:

$$z_i(t) = s_i(t) + \mathrm{j}s_i^*(t) = A_i(t)e^{\mathrm{j}\delta_i(t)} \tag{18}$$

where $A_i(t)$ and $\delta_i(t)$ are the instantaneous amplitude and instantaneous phase of $s_i(t)$ respectively:

$$\begin{cases} A_i(t) = \sqrt{s_i^2(t) + s_i^{*2}(t)} \\ \delta_i(t) = \arctan \dfrac{s_i^*(t)}{s_i(t)} \end{cases} \tag{19}$$

And the instantaneous frequency $f_i(t)$ can be obtained from the instantaneous phase $\delta_i(t)$:

$$f_i(t) = \frac{1}{2\pi} \frac{\mathrm{d}\delta_i(t)}{\mathrm{d}t} \tag{20}$$

If there is an eigenvalue $\sigma_i = -\lambda_i \pm \mathrm{j}\omega_i$, the system's oscillatory response in the time domain can be expressed as:

$$s(t) = A_{i0}e^{-\lambda_i t}\cos(\omega_i t + \varphi_{i0}) \tag{21}$$

where A_{i0}, λ_i, ω_i and φ_{i0} are initial amplitude, attenuation factor, oscillation angular frequency and phase angle respectively.

By combining Eq. (18) and Eq. (21), we can obtain:

$$\begin{cases} \ln A_i(t) = -\lambda_i t + \ln A_{i0} \\ \delta_i(t) = \omega_i t + \varphi_{i0} \end{cases} \tag{22}$$

Applying least-squares fitting to Eq. (22), the oscillation angular frequency ω_i and attenuation factor λ_i can be obtained, then the damping ratio of mode i can be calculated as:

$$\xi_i = \frac{\lambda_i}{\sqrt{\omega_i^2 + \lambda_i^2}} \tag{23}$$

Through the above analysis, the electromechanical mode parameter (the oscillation frequency f_i and the damping ratio ξ_i), can be identified from the PMU measurement data.

IV. Application of Improved FastICA in Power System Analysis

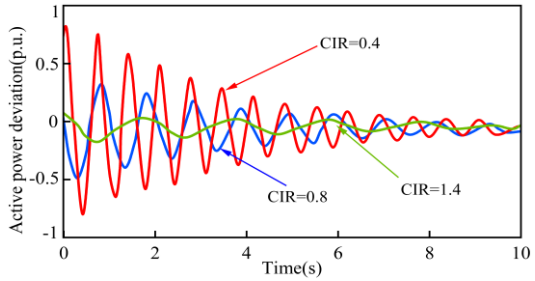

Fig. 1. Generator active power deviation.

Based on the improved FastICA described above, a scheme for identifying oscillation modes from multiple PMUs is developed, as shown in Algorithm 1 in Section IV.C. Additionally, two major challenges in its implementation process are discussed: 1) Selecting input signals based on the capacity-inertia ratio, as presented in Section IV.A; and 2) Determining the number of modal decompositions using instantaneous amplitude entropy, as discussed in Section IV.B.

A. Measurement signal selection for identifying oscillation modes based on CIR

This section further proposes a measurement signal selection strategy for determining the input signals of improved FastICA. With the aim of reliable identification, it is recommended to place PMUs at the terminals of the main generators with relatively larger rated capacities in each coherent area [26]. On the other hand, considering the uneven distribution of mode information across different measurement channels, certain critical modes can only be clearly monitored through specific signal channels. From this perspective, determining the optimal PMU measurements for mode identification can be regarded as the process of selecting measurements that provide sufficient observability for the modes of interest. The moment of inertia of a generator represents its rotor's ability to maintain its rotational state. A larger moment of inertia makes the rotor less likely to change its rotational speed and state. In other words, for different generators subjected to the same system disturbance, a generator with a large moment of inertia will exhibit slower changes in measured signals, with relatively smaller amplitude. Conversely, for a generator with a small moment of inertia, these signals change more rapidly and exhibit larger amplitudes, making it easier to observe and capture the key modes [27]. Therefore, the moment of inertia of a generator can be used as a quantitative indicator of the observability of the measurements for oscillation modes. Therefore, considering the impact of measurement reliability and measurement signal observability on mode extraction, the capacity-inertia ratio (CIR) is proposed in this section to select the input measurements, which is defined as follows:

$$\mathrm{CIR} = H / S \tag{24}$$

where H and S represents the moment of inertia and the rated capacity of the generator respectively.

In the following, the proposed CIR is briefly explained using the single-machine infinite-bus (SMIB) system as an example. The equivalent generator in SMIB is represented by the classical model with the following parameters, expressed in per

Algorithm 1: Implementation of the Improved FastICA and Modal Identification

Initialization:

1) Construct initial input matrix $\boldsymbol{X}=[x_1,x_2,\cdots,x_n]$ from multiple PMUs, apply FFT to input matrix $\boldsymbol{X}$ to obtain initial frequency matrix $\boldsymbol{\theta}$, and calculate the CIR of each generator using Eq. (24).

2) for i=1, 2, 3, ... **do**

a) Get the active power of the first i generators in CIR as the input: $\boldsymbol{X}_i=[x_1,x_2,\cdots,x_i]^{\mathrm{T}}$.

b) Calculate de-mixing matrix $\boldsymbol{W}_i$:

$$\boldsymbol{W}_i=\arg\min_{\omega}\left\|\omega\mathrm{NMP}(\omega^{\mathrm{T}}R_{i-1},\theta_i)-R_{i-1}\right\|_2^2, \text{ where}$$

$$\|\omega\|_2=1,\ R_i=\boldsymbol{X}-\sum_{k=1}^{i}a_k s_k^{\mathrm{T}}.$$

c) Get i-th IMF s_i: $s_i=\mathrm{NMP}(\boldsymbol{W}_i^{\mathrm{T}}\boldsymbol{R}_{i-1},\theta_i)$.

d) Compute IAE_i of s_i and obtain the sum of IAE_i of each IMF s_i, that is $IAE_{\mathrm{total}}(i)$:

$$IAE_i=-\sum_{t=1}^{l}p_i(t)\log_2 p_i(t)$$

$$IAE_{\mathrm{total}}(i)=\sum_{r=1}^{i}IAE_i(r),\ (r=1,2,\cdots,i)$$

e) Repeat i=i+1, recalculate $IAE_{\mathrm{total}}(i+1)$:

$$IAE_{\mathrm{total}}(i+1)=\sum_{r=1}^{i+1}IAE_{i+1}(r),\ (r=1,2,\cdots,i+1)$$

f) While $\sum_{r=1}^{i}IAE_i(r)>\sum_{r=1}^{i+1}IAE_{i+1}(r)$ is satisfied, return to **Step a)**.

end while

end for

3) Output the final de-mixing matrix $\boldsymbol{W}$: $\boldsymbol{W}=[W_1,W_2,.....,W_i]^{\mathrm{T}}$, and matrix of IMFs: $\boldsymbol{S}=[s_1,s_2,\cdots,s_i]^{\mathrm{T}}$.

4) Calculate the oscillation frequency f_i and damping ratio ξ_i:

$$f_i(t)=\frac{1}{2\pi}\frac{\mathrm{d}\delta_i(t)}{\mathrm{d}t},\ \xi_i=\frac{\lambda_i}{\sqrt{\omega_i^2+\lambda_i^2}}$$

unit on 220 MVA, 40kV base: the rated capacity (S) is 10, 5, 11p.u., and the moment of inertia is 4, 7, and 9 p.u. The corresponding CIR values are 0.4, 1.4 and 0.8. A transient three phase short-circuit fault occurs, and the active power deviation under three CIRs are obtained, as shown in Fig. 1. It is clear from Fig. 1 that as the CIR decreases, the generator active power amplitude becomes larger. Moreover, the amplitude changes more abruptly with a decrease in CIR.

Therefore, in our work, PMU measurements of generators with relatively small CIR, which means that oscillation information collected from these PMUs is more reliable and exhibits stronger observability, can be selected as the input signals for oscillation parameter identification.

B. Instantaneous Amplitude Entropy for determining the number of oscillation modes

In this section, the instantaneous amplitude entropy (IAE) is used to determine the number of modes contained in the signal, which is achieved by quantifying the complexity (i.e. the degree of information confusion) of each IMF. Its core principle is to determine the number of decomposition layers that maximize signal clarity while minimizing noise interference.

For the extracted i-th IMF ($s_i(t)$) in Section III.A, the instantaneous amplitude $A_i(t)$ is obtained by using HT. And the normalized probability distribution of $A_i(t)$ is calculated as [28]:

$$p_i(t)=A_i(t)/\sum_{t=1}^{l}A_i(t) \tag{25}$$

where $p_i(t)$ is the normalized probability distribution of $A_i(t)$; l is the length of the oscillation signal.

Furthermore, calculate the instantaneous amplitude entropy of each component (IAE_i), which is as follows:

$$IAE_i=-\sum_{t=1}^{l}p_i(t)\log_2 p_i(t) \tag{26}$$

The sum of IAE_i under different modes K is calculated:

$$IAE_{\mathrm{total}}(K)=\sum_{i=1}^{K}IAE_i \tag{27}$$

According to the essential characteristics of IAE, we can analyze that: when the decomposed signal is dominated by a single pattern, its instantaneous amplitude varies more simply, resulting in a lower IAE; Conversely, if the decomposed signal is mixed, meaning it contains multiple patterns, its instantaneous amplitude variation becomes more complex, leading to a higher IAE. Therefore, details for determining the number of oscillation modes are elaborated as follows:

1) When the number of decomposition K is smaller than the true number of decomposition modes K_{opt} (K<K_{opt}), some decomposed IMFs may contain multiple modes, resulting in a relatively large IAE.

2) When K=K_{opt}, the PMU measurements are decomposed into K_{opt} single-mode IMFs, and the IAE reaches its minimum value.

3) When K is greater than K_{opt}, over-decomposition occurs, causing noise to be separated into redundant modes. Consequently, the IAE increases compared to the case when K=K_{opt}, meaning the IAE value rebounds.

Finally, by analyzing the variation trend of the total IAE (IAE_{total}) with respect to the number of decomposition modes K, the lowest point of the variation curve can be identified, representing the actual number of modes contained in the measurement data.

C. Framework of the Proposed Method

Following the representation above, when suitable measured input signals are selected and the number of oscillation modes is determined, the framework of the proposed method for identifying oscillation modes from PMU measurement is presented in **Algorithm 1.**

V. SIMULATION AND ANALYSIS

In this section, case studies based on the synthetic signal, the IEEE 16-machine 5-area test system and actual measurement data are adopted to investigate the performance of the proposed method. Moreover, the EMD, VMD, as well as conventional FastICA methods, are applied to the same oscillation signals for comparison.

A. Synthetic signal

This section constructs a synthetic signal matrix $\boldsymbol{X}$, which is generated by mixing the three source signals in Eq. (28).

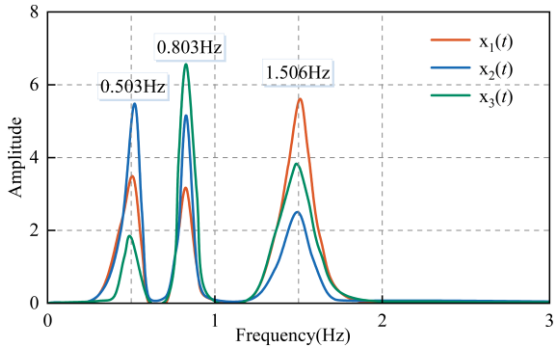

Fig. 2. FFT spectra of the synthetic signal.

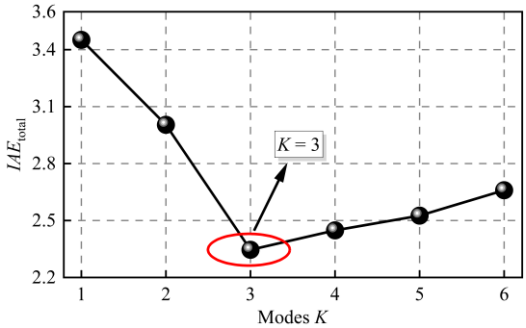

Fig. 3. Results of the IAE_{total}

$$\begin{cases} s_1(t) = 15e^{-0.2t}\cos(0.8\times 2\pi t) \\ s_2(t) = 6e^{-0.3t}\cos(0.5\times 2\pi t) \\ s_3(t) = 6e^{-0.3t}\cos(1.5\times 2\pi t + \pi/3) \end{cases} \tag{28}$$

The synthetic signal matrix $\boldsymbol{X}$ can be linearly represented by Eq. (29), and Gaussian white noise with the signal-to-noise ratio (SNR) of 30 dB is added.

$$\underbrace{\begin{pmatrix} x_1(t) \\ x_2(t) \\ x_3(t) \end{pmatrix}}_{\boldsymbol{X}} = \boldsymbol{A}\cdot \underbrace{\begin{pmatrix} s_1(t) \\ s_2(t) \\ s_3(t) \end{pmatrix}}_{\boldsymbol{S}} = \begin{Bmatrix} 0.63*s_1(t) - 0.48*s_2(t) + 0.61*s_3(t) \\ 0.34*s_1(t) + 0.88*s_2(t) + 0.33*s_3(t) \\ 0.7*s_1(t) - 0.72*s_3(t) \end{Bmatrix} \tag{29}$$

where $\boldsymbol{A}$ is the 3×3 order-mixing matrix and is orthogonal, satisfying $\boldsymbol{A}.\boldsymbol{A}^{\mathrm{T}} = \boldsymbol{I}$, $\boldsymbol{I}$ is the identity matrix [29].

To accurately obtain the initial frequencies of improved FastICA, FFT spectrum analysis is performed on the oscillation signals, and the spectrum results are shown in Fig.2. It can be observed from the figure that the synthetic signal contains three oscillation modes with frequencies of 0.503 Hz, 0.803 Hz and 1.506 Hz respectively. Therefore, the initial frequencies are determined to be 0.503 Hz, 0.803 Hz and 1.506 Hz.

To avoid the influence of measurement noise and non-stationary characteristics on the FFT spectrum, IAE is used to assist the FFT in accurately determining the initial frequencies of improved FastICA. According to Section IV.B, the results of IAE_{total} for different modes values K are shown in Fig.3. It can be observed that as K increases, the total entropy IAE_{total} initially decreases. However, when K increases further, the IAE_{total} starts to increase again. When K is equal to 3, the IAE_{total} reaches its minimum value. Therefore, the number of oscillation modes is determined to be 3.

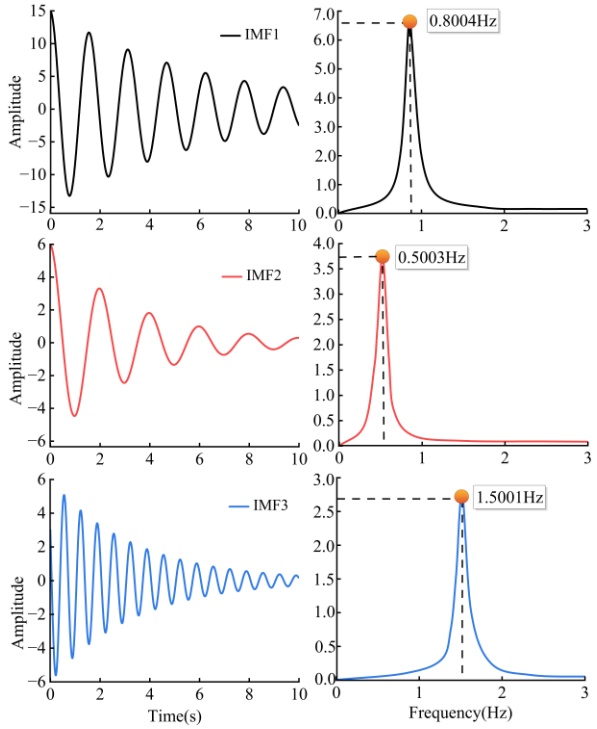

Fig. 4. Decomposition results of the proposed method and FFT spectra.

TABLE I
IDENTIFICATION RESULTS OF IMPROVED FASTICA

	Analytical value	Improved FastICA	Absolute Error
Fre (Hz)	0.8	0.8004	0.0004
	0.5	0.5003	0.0003
	1.5	1.5001	0.0001
Damp (%)	3.97	4.05	0.08
	9.51	9.58	0.07
	3.18	3.27	0.09

Based on the initial frequencies (0.503Hz, 0.803Hz, and 1.506Hz), the proposed improved FastICA is used to identify the oscillation parameters. The decomposition results are shown in Fig. 4, and the parameter identification results using HT are listed in Table I. It should be note that "Fre" and "Damp" here correspond to frequency and damping ratio respectively, and the abbreviation will be used in the subsequent tables. It can be seen from Table I and Fig. 4 that the signal is decomposed into three IMFs by the proposed method. Meanwhile, the identified oscillation frequencies and damping ratios are consistent with those of the original signals, with the maximum absolute errors in frequency and damping ratio being 0.0004 Hz and 0.09% respectively. The excellent decomposition capability of the proposed method ensures relatively small errors in the parameter identification, further illustrating the decomposition accuracy and effectiveness of the improved FastICA method.

To verify the robustness of the proposed method to the initial frequencies, this paper decomposes the synthetic signal using three different sets of initial frequencies as follows: 1) 0.503Hz, 0.803Hz, 1.506Hz (FFT spectra results from Fig. 2); 2) 0.3Hz, 1.0Hz, 1.8Hz and 3) 1.3Hz, 2.3Hz, 2.5Hz. The absolute errors of the damping ratio and frequency identification results are shown in Fig. 5. In Fig. 5, by comparing the identification

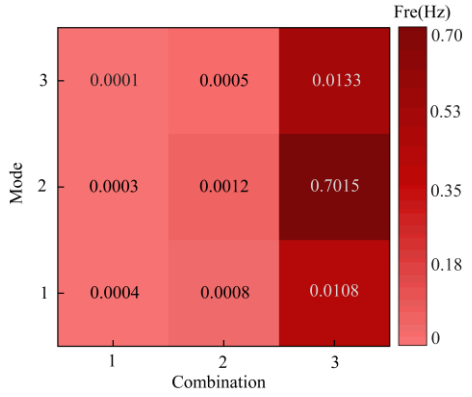

Fig. 5. Absolute error (a) Frequency. (b) Damping ratio.

TABLE II
IDENTIFICATION RESULTS OF DIFFERENT METHODS

Method	Mode	Fre (Hz)	Absolute Error (Hz)	Damp (%)	Absolute Error (%)
Analytical value	1	0.8	-	3.97	-
	2	0.5	-	9.51	-
	3	1.5	-	3.18	-
Improved FastICA	1	0.8004	0.0004	4.05	0.08
	2	0.5003	0.0003	9.58	0.07
	3	1.5001	0.0001	3.27	0.09
FastICA	1	0.8006	0.0006	4.13	0.16
	2	0.5006	0.0006	9.71	0.20
	3	1.5002	0.0002	3.29	0.11
EMD	1	0.84	0.04	3.41	0.56
	2	0.47	0.03	8.06	1.45
	3	1.48	0.02	3.06	0.12
	4	0.12	-	5.21	-
VMD	1	0.8005	0.0005	4.10	0.13
	2	0.5005	0.0005	9.70	0.19
	3	1.5005	0.0005	3.28	0.10

results of the 1st and the 2nd groups, it can be known that the identification results of both groups remain relatively close to the analytical values. Specifically, the maximum absolute errors of oscillation frequency and damping ratio are within 0.01 Hz and 0.2% respectively. Next, by comparing the identification results of the 1st and the 3rd groups, it can be observed that among the three oscillation modes, the frequency identification of Mode 2 exhibits the largest deviation from the true value, with the absolute error of 0.7015 Hz, which indicates a significant false mode phenomenon. Regarding the damping ratio identification results, the absolute errors for Mode 1 and Mode 2 are relatively large, which are 1.01% and 0.96%

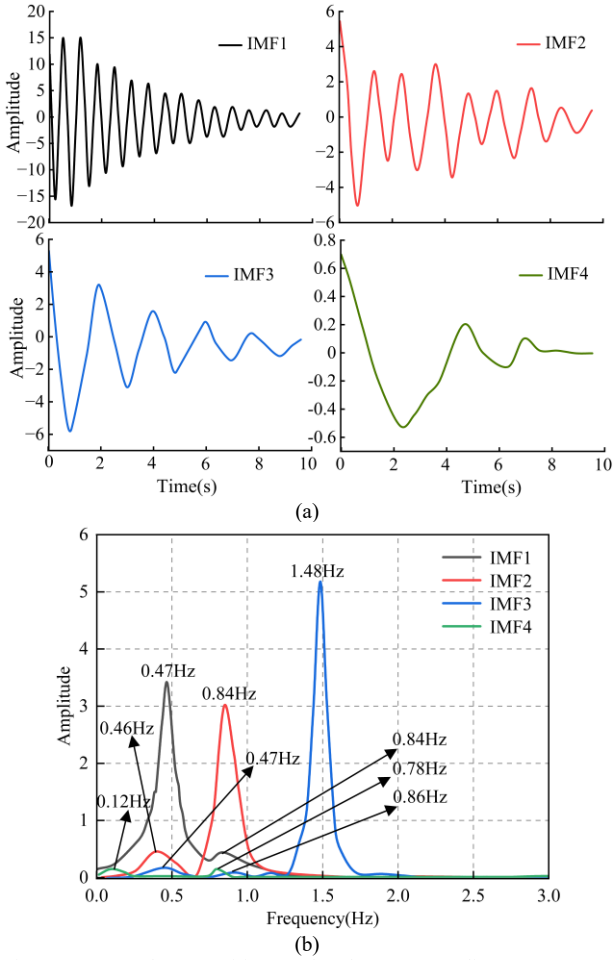

Fig. 6. (a) EMD decomposition results. (b) Corresponding IMF spectra.

respectively. Through the comparative analysis, it can be found that the significant deviation in the 3rd group's results can be attributed to the initial frequency differing greatly from the true frequency, with a maximum deviation of 1.5Hz. Such a large deviation leads to errors in the proposed method when solving the minimization problem. Therefore, an appropriate initial frequency needs to be determined to ensure the accuracy of the identification results.

With the aim of verifying the superiority of the proposed method in improving mode mixing, EMD, VMD and conventional FastICA are used to perform signal decomposition on the same signal, with the HT used to identify the mode parameters. The oscillation frequency and damping ratio results are shown in Table II. From Table II, it can be known that the proposed method, VMD, and the FastICA can accurately identify the oscillation frequency, with their identification accuracies being comparable and all within 0.01 Hz. However, regarding the damping ratio, the proposed method maintains high identification accuracy. In contrast, for VMD and the conventional FastICA, slight mode mixing occurs, leading to larger errors in the damping ratio identification results, with maximum errors of 0.19% and 0.20% respectively.

Compared with the aforementioned three methods, the mode mixing in the EMD method is the most severe, resulting in the maximum absolute errors in frequency and damping ratio

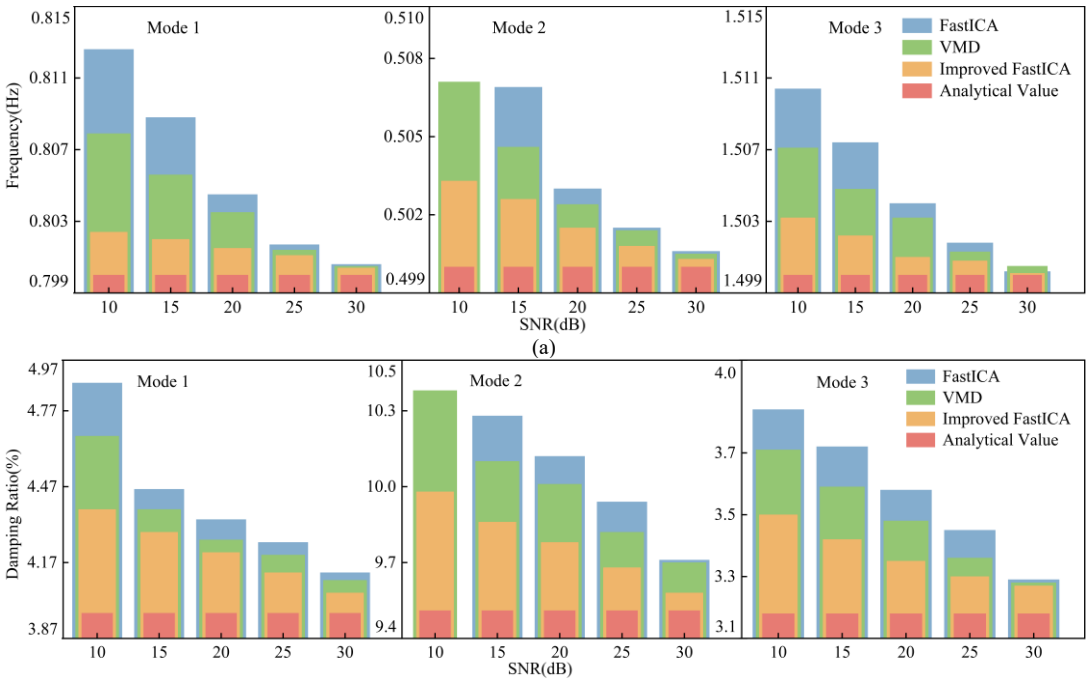

Fig. 7. Identification results under different SNRs (a) Frequency; (b) Damping ratio.

identification are 0.04 Hz and 1.45% respectively. Moreover, the Mode 4 in the identification results is not included in the analytical values, which can be considered as a false mode. In particular, the IMFs of EMD and the corresponding spectra are shown in Fig. 6(a) and Fig. 6(b), while the residual component is not displayed. From Fig. 6(a) and Fig. 6(b), it can be found that all four IMFs exhibit non-monotonic and irregular fluctuations to varying degrees. Notably, for the 4th IMF, it contains frequencies of 0.12 Hz and 0.78 Hz, and 0.12 Hz is not included in the synthetic signal and is a typical spurious mode. The above analysis indicates that the proposed method effectively avoids mode mixing in signal decomposition, providing single-frequency IMFs for the subsequent extraction of oscillation parameters through the HT.

In order to verify the robustness of the proposed method against noise, the noise intensity gradually increased from the initial 30dB by adding Gaussian white noise at levels of 25dB, 20dB, 15dB, and 10dB to the same signal. The improved FastICA, VMD and the conventional FastICA are used for signal decomposition, the identification results obtained through the HT are shown in Fig. 7. EMD exhibits severe mode mixing when SNR is 30dB, due to space limitations, the noise resistance analysis of EMD will not be included.

It is obvious from Fig. 7 that under different noise conditions, identification errors of the conventional FastICA method are the largest, followed by those of the VMD method. Notably, when the SNR is 10dB, conventional FastICA fails to identify Mode 2. And the bar chart of the proposed method is closer to the theoretical values compared to those of the VMD and conventional FastICA methods. Moreover, as noise intensity increases, the accuracy of identification results of the proposed method decreases much less than that of the other two methods. The identification results further indicates that the proposed method has strong robustness to noise, and outperforms both the VMD and conventional FastICA methods.

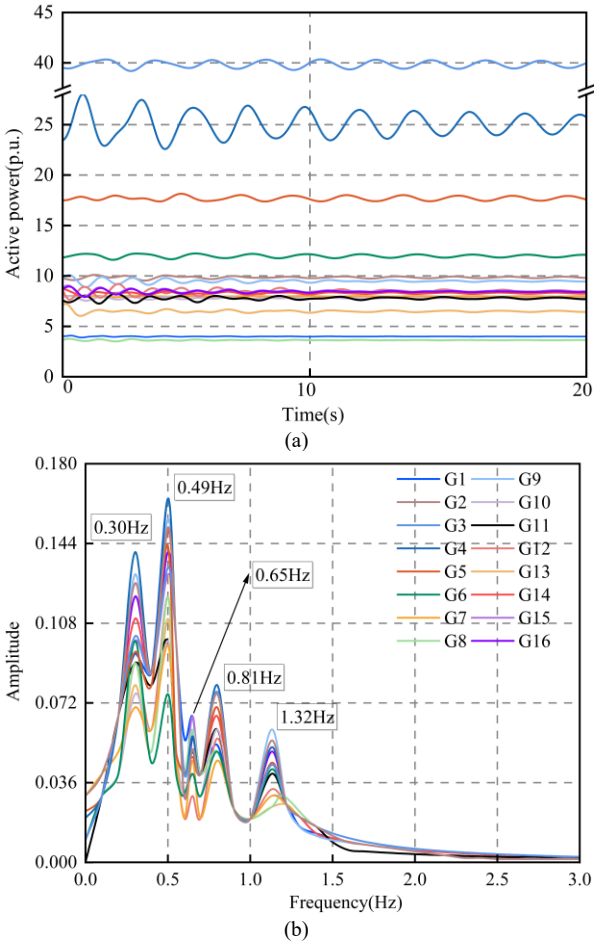

Fig. 8. (a) Generator active power. (b) Corresponding FFT spectra.

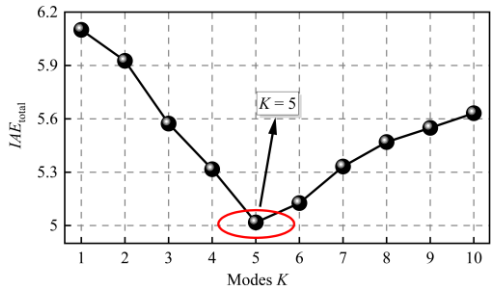

Fig. 9. Results of the IAE_{total}

TABLE III
GENERATOR PARAMETERS AND CORRESPONDING CIR

	Rated capacity (p.u.)	Moment of Inertia (p.u.)	CIR
G11	16	4.1	0.256
G13	19	5.9	0.311
G8	10	4.1	0.410
G6	10	4.4	0.440
G2	10	4.79	0.479
G12	12	7.4	0.617
G7	8	5.66	0.708
G16	11	7.8	0.709
G3	8	5.7	0.712
G4	8	5.69	0.712
G5	7	5.4	0.771
G10	12	9.37	0.781
G14	9	7.3	0.811
G9	8	6.56	0.820
G15	8	6.7	0.838
G1	3	12.6	4.200

B. 16-machine 5-area test system

In this section, simulation data from the IEEE 16-machine 5-area system is used to evaluate the applicability of the proposed method in a large-scale power system. Detailed parameters of the 16-generator system can be found in [30]. A representative contingency is considered: a 3-phase permanent fault occurred at bus 16 with a duration of 0.1s. Fig.8 shows the active power of all the generators, with the sampling frequency set to 100Hz. And the 30dB white noise is added to the active power.

To determine the initial frequency, spectrum analysis is also performed on the measured signals, and the FFT results are shown in Fig. 8. As shown in Fig. 8, there are four distinct peaks, with frequencies of approximately 0.30Hz, 0.49Hz, 0.81Hz, and 1.32Hz. In addition, a mode with an insignificant peak at 0.65Hz requires further analysis using IAE to determine whether it represents an actual oscillation mode. The results of $IAE_{total}(K)$ under different K values are shown in Fig. 9. It is clear from Fig. 9 that, when $K = 5$, the value of IAE_{total} reaches its minimum. Therefore, it is determined that the oscillation signal contains five modes, with initial frequencies of 0.30Hz, 0.49Hz, 0.65Hz, 0.81Hz and 1.32Hz.

After determining the initial frequency, the proposed method is used to identify oscillation parameters. Moreover, the capacity-inertia ratio (CIR) index, proposed in Section IV.A, is used to select the required input signals. The CIR results of the sixteen generators are shown in Table III.

To further validate the effectiveness of the proposed CIR for signal selection, a comparative analysis was conducted using three different combinations, which are as follows: 1) G11, G13, G8, G6, G2; 2) G1, G15, G9, G14, G10 and 3) G11, G12, G5, G1, G13. Table IV shows the comparative identification results for all five oscillation modes using the proposed method, conventional FastICA, EMD and VMD, with small signal stability analysis (SSSA) as the reference under the three combinations. For clear visualization, the identification results of the proposed method are shown in Fig. 10, while the decomposition results and the corresponding FFT results under the first group are shown in Fig. 11.

From Table IV and Fig. 10, the results indicate that for all four identification methods, compared with the second and third groups, the generator combination with the smallest CIR (the

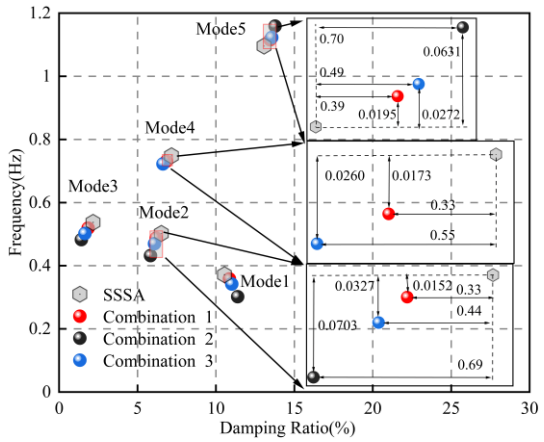

Fig. 10. Calculation results under different CIR.

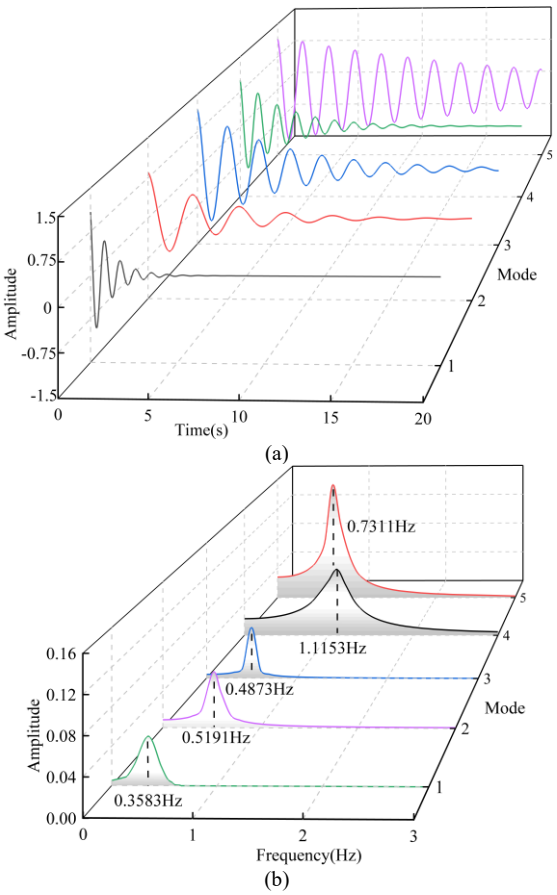

Fig. 11. (a) Decomposition results of the improved FastICA. (b) Corresponding FFT spectra.

TABLE IV
IDENTIFICATION RESULTS UNDER THREE COMBINATIONS

Combination	Mode	Fre (Hz)					Damp (%)				
		SSSA	Improved FastICA	FastICA	EMD	VMD	SSSA	Improved FastICA	FastICA	EMD	VMD
1	1	0.3717	0.3583	0.3335	0.4133	0.3260	10.55	10.86	11.06	11.42	10.99
	2	0.5025	0.4873	0.4598	0.5963	0.4701	6.52	6.19	5.92	7.60	5.95
	3	0.5375	0.5191	0.4853	0.4267	0.4746	2.17	1.85	1.55	5.63	1.66
	4	0.7484	0.7311	0.7097	-	0.7071	7.17	6.84	6.54	-	6.64
	5	1.0958	1.1153	1.1422	1.4778	1.1583	13.07	13.46	13.72	8.55	13.68
2	1	0.3717	0.3021	0.2981	0.4921	0.3011	10.55	11.39	11.52	11.92	11.48
	2	0.5025	0.4322	0.4013	0.6542	0.4157	6.52	5.83	5.49	7.93	5.43
	3	0.5375	0.4825	-	-	-	2.17	1.42	-	-	-
	4	0.7484	-	-	-	-	7.17	-	-	-	-
	5	1.0958	1.1589	1.2001	1.6984	1.1820	13.07	13.77	14.01	8.02	14.08
3	1	0.3717	0.3419	0.3118	0.4389	0.3107	10.55	11.01	11.22	11.63	11.14
	2	0.5025	0.4698	0.4412	0.6103	0.4559	6.52	6.08	5.81	7.72	5.79
	3	0.5375	0.5020	0.4661	0.4025	0.4601	2.17	1.65	1.38	5.81	1.43
	4	0.7484	0.7224	0.6924	-	0.6821	7.17	6.62	6.39	-	6.31
	5	1.0958	1.1230	1.1702	1.4943	1.1691	13.07	13.56	13.81	8.34	13.77

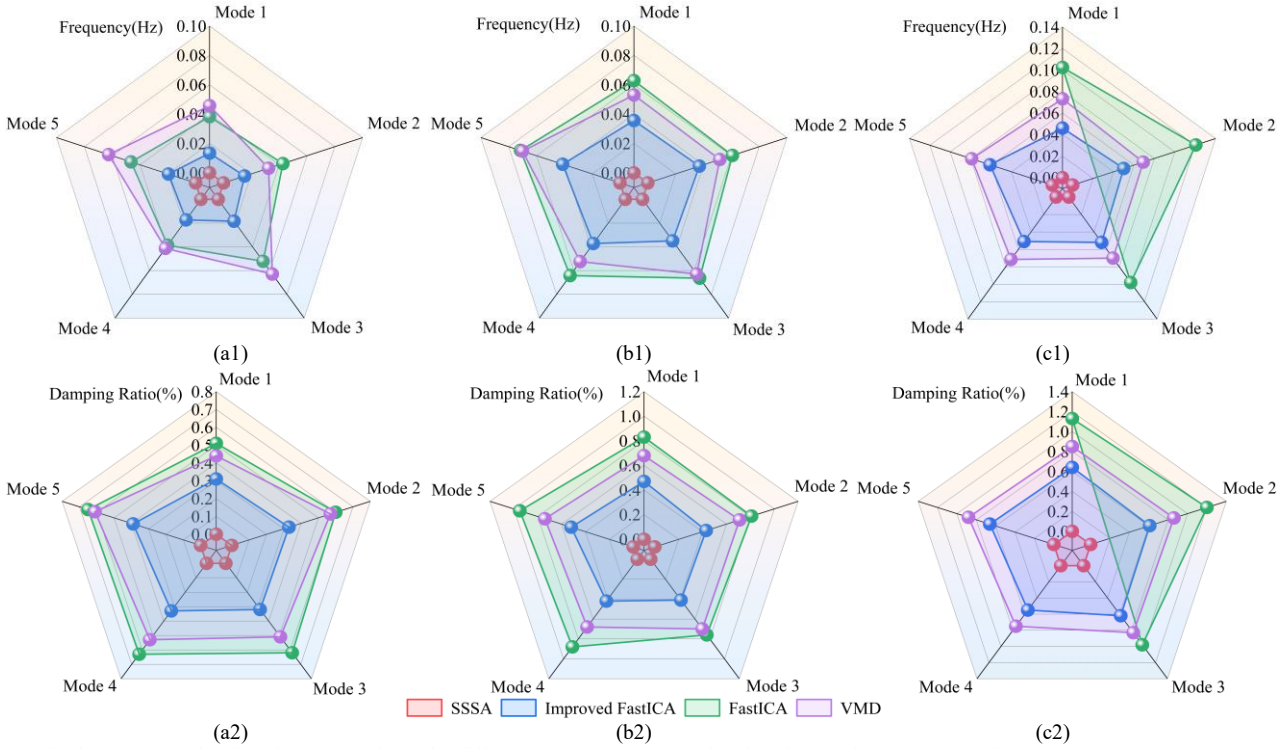

Fig.12. Absolute errors in the identification results under different SNRs. (a1) (a2) 30 dB; (b1) (b2) 20 dB; (c1) (c2) 10 dB

first group) produces oscillation frequency and damping ratio results that are much closer to the SSSA results. Using the first group as inputs, the proposed method achieves maximum absolute errors of 0.0195Hz for frequency and 0.39% for damping ratio. Especially, when using the second generator combination, the proposed method fails to identify Mode 4, resulting in mode omission. Meanwhile, the results in Table IV also show that the proposed method achieve higher accuracy than the other three method. In contrast, even when using the active power of generators G11, G13, G8, G6 and G2 as inputs, the EMD still has mode aliasing, the maximum frequency and damping ratio errors reach 0.3820Hz and 4.52% respectively, and the mode omission (Mode 4) occurs. Especially, the FastICA, VMD and EMD methods even fails to identify Mode 3 and Mode 4 under the second generator combination, resulting in mode omission. The above analysis fully validates the effectiveness of the proposed CIR index in selecting generators for mode identification, as well as the superiority of the proposed method in identifying oscillation parameters.

Next, the SNR was reduced from the initial 30dB to 20dB and 10 dB to verify the superiority of the proposed method in terms of noise resistance. The absolute errors of the identification results under different SNRs are shown in Fig.12. Fig. 12 shows that under different SNRs, the identification accuracy of the proposed method is the best, followed by the VMD method. As noise intensity increases, the identification accuracy of the conventional FastICA method declines significantly. In particular, when the SNR drops to 10 dB, the conventional FastICA method fails to identify Mode 4 and Mode 5. The above analysis demonstrates that the proposed method is robust and highly adaptable to noise, ensuring accurate identification of oscillation parameters.

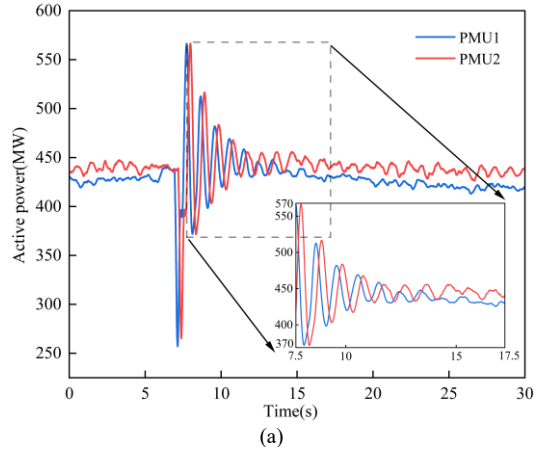

(a)

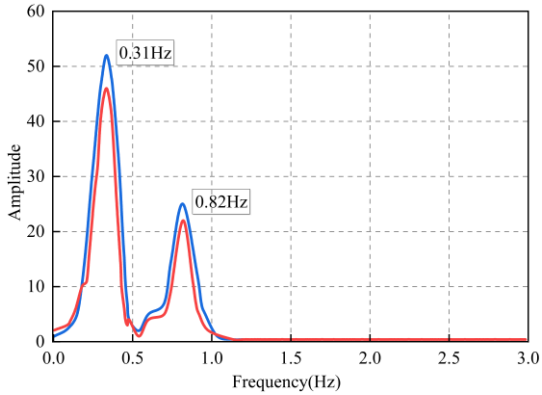

(b)

Fig. 13. (a) Generator active power. (b) Corresponding FFT spectra.

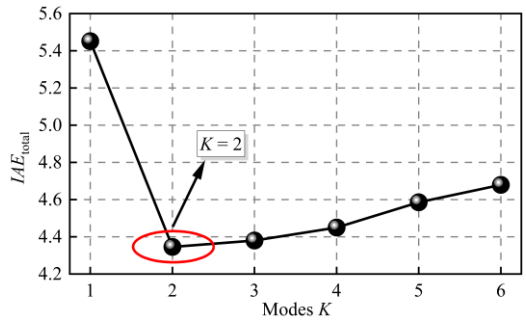

Fig. 14. Results of the IAE_{total}

C. Actual measurement data

This section takes actual measurement data as an example to test the performance of the proposed method in oscillation mode decomposition. The measurement data in this study was recorded by PMUs during a real event in Northeast China power grid. The PMU measurements was recorded for a duration of approximately 30s with a sampling frequency of 100 Hz. The active power data during the oscillation of two generators are plotted in Fig. 13(a), and the oscillation data of 7.5s-17.5s are selected for analysis.

The initial frequency of the proposed method identified through FFT in Fig. 13(b) are approximately 0.31Hz and 0.82Hz respectively. Moreover, the results of $IAE_{\text{total}}(K)$ in Fig. 14 show that when K = 2, the value of IAE_{total} reaches its minimum, and the mode values K is consistent with the FFT results. Consequently, the initial frequencies are determined as 0.31Hz and 0.82Hz.

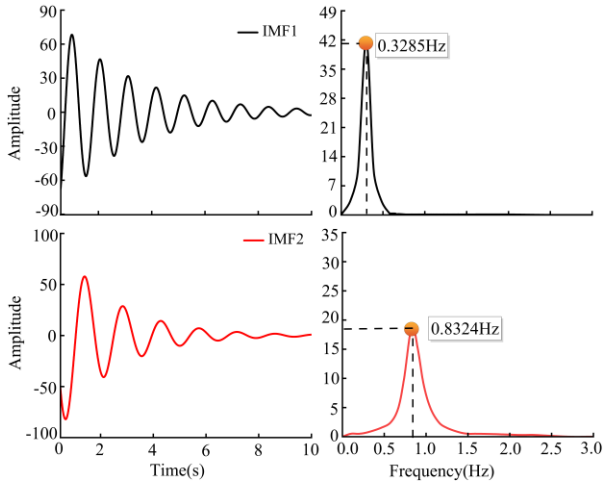

Fig. 15. Decomposition results of the proposed method and FFT spectra.

TABLE V
IDENTIFICATION RESULTS OF DIFFERENT METHODS

	Mode	Prony	Improved FastICA	Absolute Error
Fre (Hz)	1	0.2921	0.3285	0.0364
	2	0.8035	0.8324	0.0289
Damp (%)	1	3.88	4.12	0.24
	2	8.13	8.45	0.32

Subsequently, using the identified initial frequencies, the proposed method is applied to the active power data from two generators to extract oscillation parameter. The identification results are shown in Table V, and the single-frequency decomposition results are shown in Fig.15. From Table V and Fig. 15, it can be observed that the proposed method successfully decomposes the signal into two single-frequency mode components. Moreover, the frequency of each component is consistent with the FFT results from Fig. 13(b). The Prony results are also listed in Table V. The modal estimation results of the proposed method are quite close to those by Prony, the maximum absolute errors in frequency and damping ratio reach only 0.0364Hz and 0.32% respectively. The above results show that the proposed method achieves great identification results for the analysis of actual measurements, further demonstrating the accuracy and efficacy of the proposed method.

VI. CONCLUSION

This paper proposes an improved FastICA-based method for identifying electromechanical oscillation using synchronized measurements from multiple PMUs. The NMP is employed to enable the conventional FastICA method to achieve reliable mode identification performance from polluted noise-contaminated data. The performance of the proposed method is evaluated using the synthetic signal, simulation data of the IEEE 16-machine 5-area test system and actual measurement data. The simulation results demonstrate the identification accuracy of oscillation frequency and damping ratio from noise-containing synchrophasor measurement of the proposed method, thereby enables the applications of FastICA for modes identification with noise-polluted data. Compared with

conventional FastICA, EMD and VMD methods, the proposed method exhibits superior performance in improving mode aliasing and strong robustness to noise. Besides, a comparative analysis of the proposed method with the other three methods under different input signals is also conducted. The comparative results show that the CIR-based signal selection strategy simplifies the measurement signals while preserving essential electromechanical mode information, preventing mode loss due to input reduction. Future work will focus on adapting the proposed method to different measured data, such as ambient data.

ACKNOWLEDGMENT

This study is supported by the State Key Laboratory of Alternate Electrical Power System with Renewable Energy Sources (Grant No. LAPS24014)

REFERENCES

[1] Y. Hu, S. Bu, S. Yi, J. Zhu, J. Luo, and Y. Wei, "A novel energy flow analysis and its connection with modal analysis for investigating electromechanical oscillations in multi-machine power systems," *IEEE Trans. Power Syst*., vol. 37, no. 2, pp. 1139–1150, Mar. 2022.

[2] V. E. Rudnik, R. A. Ufa, and Y. Y. Malkova, "Analysis of low-frequency oscillation in power system with renewable energy sources," *Energy Reports*, vol. 8, no. 9, pp. 394–405, Nov. 2022.

[3] M. Zuhaib and M. Rihan, "Identification of low-frequency oscillation modes using PMU based data-driven dynamic mode decomposition algorithm," *IEEE Access*, vol. 9, pp. 49434–49446, Mar. 2021.

[4] H. Li, C. Lu, C. Fei, Y. Hu, B. Huang, and L. Yuan, "Full-parameters identification technique of attenuated oscillations in power system monitoring," in 2021 Global Reliability and Prognostics and Health Management (*PHM*-Nanjing), Nanjing, China: IEEE, Oct. 2021, pp. 1–5.

[5] M. Khodadadi Arpanahi, M. Kordi, R. Torkzadeh, H. Haes Alhelou, and P. Siano, "An augmented prony method for power system oscillation analysis using synchrophasor data," *Energies*, vol. 12, no. 7, pp. 1267, Apr. 2019.

[6] R. Tapia-Olvera, D. Guillen, F. Beltran-Carbajal, and L. M. Castro, "An adaptive scheme to improve prony's method performance to estimate signal parameters of power system oscillations," *IEEE Trans. Instrum. Meas*., vol. 71, pp. 1–12, Jul. 2022.

[7] Z. Duan, Y. Meng, S. Yan, Y. Duan, X. Wang, and X. Wang, "Large-signal stability analysis for offshore wind power fractional frequency transmission system with modular multilevel matrix converter," *Int. J. Electr. Power Energy Syst.,* vol. 153, pp. 109379, Nov. 2023.

[8] C. Liu, F. Zhuo, and F. Wang, "Fault diagnosis of commutation failure using wavelet transform and wavelet neural network in HVDC transmission system," *IEEE Trans. Instrum. Meas*., vol. 70, pp. 1–8, Sep. 2021.

[9] T. Jin, S. Liu, and R. C. C. Flesch, "Mode identification of low-frequency oscillations in power systems based on fourth-order mixed mean cumulant and improved TLS-ESPRIT algorithm," *IET Gener. Transm. Distrib.*, vol. 11, no. 15, pp. 3739–3748, Oct. 2017.

[10] H. Li, S. Bu, J. Wen, and C. Fei, "Synthetical modal parameters identification method of damped oscillation signals in power system," *Applied Sciences*, vol. 12, no. 9, pp. 4668, May 2022.

[11] S. You, J. Guo, G. Kou, Y. Liu, and Y. Liu, "Ambient PMU data-based system oscillation analysis using multivariate empirical mode decomposition," *Electr Pow Syst. Res.*, vol. 134, pp. 158–166, May 2016.

[12] D. Yang, J. Tian, L. Wang, G. Cai, J. Ma, and B. Wang, "Optimal mode decomposition-based analysis of electromechanical oscillations of power systems using synchrophasors," *IEEE Access*, vol. 8, pp. 192408–192418, Oct. 2020.

[13] Y. Zhao, J. Zhang, and Q. Zhao, "Online monitoring of low-frequency oscillation based on the improved analytical modal decomposition method," *IEEE Access*, vol. 8, pp. 215256–215266, Nov. 2020.

[14] P. Cao, H. Wang, and K. Zhou, "Multichannel signal denoising using multivariate variational mode decomposition with subspace projection," *IEEE Access*, vol. 8, pp. 74039–74047, Apr. 2020.

[15] J. G. Philip and T. Jain, "An improved stochastic subspace identification based estimation of low frequency modes in power system using synchrophasors," *Int. J. Electr. Power Energy Syst.*, vol. 109, pp. 495–503, Jul. 2019.

[16] K. K. Anaparthi, B. Chaudhuri, N. F. Thornhill, and B. C. Pal, "Coherency identification in power systems through principal component analysis," *IEEE Trans. Power Syst.*, vol. 20, no. 3, pp. 1658-1660, Aug. 2005.

[17] L. Cai, N. F. Thornhill, S. Kuenzel, and B. C. Pal, "Wide-area monitoring of power systems using principal component analysis and *k*-nearest neighbor analysis," *IEEE Trans. Power Syst*., vol. 33, no. 5, pp. 4913–4922, Sep. 2018.

[18] D. Li and J. Zhang, "Feature intelligent generation based on quantum computing and variational independent component analysis for nonstationary weak fault diagnosis," *IEEE Trans. Instrum. Meas*., vol. 74, pp. 1–12, Apr. 2025.

[19] S. M. Hirsh, B. W. Brunton, and J. N. Kutz, "Data-driven spatiotemporal modal decomposition for time frequency analysis," *Appl. Comput. Harmon. Anal.*, vol. 49, no. 3, pp. 771–790, Nov. 2020.

[20] A. Q. Zhang, L. L. Zhang, M. S. Li, and Q. H. Wu, "Identification of dominant low frequency oscillation modes based on blind source separation," *IEEE Trans. Power Syst*., vol. 32, no. 6, pp. 4774–4782, Nov. 2017.

[21] M. Chang, X. Wang, X. Lv, and R. Kong, "Modeling and low-frequency oscillation analysis of an asymmetrical traction power system connected to power grid," *IEEE Trans. Transp. Electrific*., vol. 9, no. 1, pp. 1750–1764, Mar. 2023.

[22] C. A. Musluoglu and A. Bertrand, "Distributed blind source separation based on FastICA," *IEEE Signal Process. Lett*., vol. 32, pp. 881–885, 2025.

[23] C. Liu, Z. Shi, and T. Y. Hou, "On the uniqueness of sparse time-frequency representation of multiscale data," *Multiscale Model. Simul*., vol. 13, no. 3, pp. 790–811, Jan. 2015.

[24] T. Y. Hou and Z. Shi, "Data-driven time–frequency analysis," *Appl. Comput. Harmon. Anal.*, vol. 35, no. 2, pp. 284–308, Sep. 2013.

[25] L. Zao and R. Coelho, "On the estimation of fundamental frequency from nonstationary noisy speech signals based on the Hilbert–Huang transform," *IEEE Signal Process. Lett*., vol. 25, no. 2, pp. 248–252, Feb. 2018.

[26] D. Yang, G. Cai, and K. Chan, "Extracting inter-area oscillation modes using local measurements and data-driven stochastic subspace technique," *J. Mod. Power Syst. Clean Energy*, vol. 5, no. 5, pp. 704–712, Sep. 2017.

[27] L. Wang et al., "Dominant inter-area oscillation mode identification using local measurement and modal energy for large-scale power systems with high grid-tied VSCs penetration," *Int. J. Electr. Power Energy Syst.*, vol. 117, pp. 105697, May 2020.

[28] M. Civera and C. Surace, "An application of instantaneous spectral entropy for the condition monitoring of wind turbines," *Applied Sciences*, vol. 12, no. 3, pp. 1059, Jan. 2022.

[29] A. Tharwat, "Independent component analysis: An introduction," *Appl. Comput. Inform*., vol. 17, no. 2, pp. 222–249, Apr. 2021.

[30] C. Canizares et al., "Benchmark models for the analysis and control of small-signal oscillatory dynamics in power systems," *IEEE Trans. Power Syst*., vol. 32, no. 1, pp. 715–722, Jan. 2017.

Lixin Wang received the B. S., M. S. and Ph.D. degrees from Northeast Electric Power University, Jilin, China, in 2014, 2017 and 2021 respectively, then worked as a Postdoctoral Fellow there in 2024 and 2025. She was also a Visiting Scholar at Auckland University of Technology, Auckland, New Zealand, in 2025.

Her research interests include power system stability analysis and control, and data-driven situational awareness for renewable power system.

Binyan Wang received the B.S. degree from Northeast Electric Power University, Jilin, China, in 2023, where he is currently pursuing the M.S. degree.

His research interests include power system stability analysis and control.

Han Gao received the B.S. and Ph.D. degrees from Northeast Electric Power University, Jilin, China, in 2017 and 2023, respectively.

Her research interests include machine learning, and data-driven power system stability analysis and control.

Deyou Yang (Member, IEEE) received the B.S. and M.S. degrees from Northeast Electric Power University, Jilin, China, in 2005 and 2009, respectively, and the Ph.D. degree from North China Electric Power University, Beijing, China, in 2014.

From 2009 to 2010, he was a Research Assistant (RA) with Hong Kong Polytechnic University, Hong Kong. He is currently a Professor of electrical engineering with Harbin University of Science and Technology (HUST), Harbin, China. His research interests include power system stability analysis and control.

Shiwei Xia received the Ph.D. degree in power system and its automation from The Hong Kong Polytechnic University, Hong Kong, China, in 2015, then worked as a Postdoctoral Fellow there in 2016 and 2017. He was also a Visiting Scholar in the Robert W. Galvin Center for Electricity Innovation at Illinois Institute of Technology, Chicago, USA, in 2019.

He is currently an Associate Professor at North China Electric Power University, Beijing, China. His research interests include renewable power system operation and control.

Tek Tjing Lie (Senior Member, IEEE) received the B.S. degree in electrical engineering from Oklahoma State University, Stillwater, OK, USA, in 1986 and the M.S. and Ph.D. degrees in electrical engineering from Michigan State University, East Lansing, MI, USA, in 1988 and 1992 respectively.

He is currently a Full Professor and the Head of the School of Engineering, Computer and Mathematical Sciences at Auckland University of Technology, Auckland, New Zealand. He was the Chair of the IEEE New Zealand North Section from 2020 to 2023 and as Vice-Chair in 2024. His research interests include power system operation and control, deregulated electrical power markets, AI applications to power systems, power electronics, renewable energy, and smart grids.